Journal for ImmunoTherapy of Cancer

Expression of KLRG1 and CD127 defines distinct CD8$^+$ subsets that differentially impact patient outcome in follicular lymphoma

Hongyan Wu,[1] Xinyi Tang,[2] Hyo Jin Kim,[2] Shahrzad Jalali,[2] Joshua C Pritchett,[2] Jose C Villasboas,[2] Anne J Novak,[2] Zhi-Zhang Yang ,[2] Stephen M Ansell[2]

To cite: Wu H, Tang X, Kim HJ, *et al*. Expression of KLRG1 and CD127 defines distinct CD8$^+$ subsets that differentially impact patient outcome in follicular lymphoma. *Journal for ImmunoTherapy of Cancer* 2021;**9**:e002662. doi:10.1136/jitc-2021-002662

► Additional supplemental material is published online only. To view, please visit the journal online (http://dx.doi.org/10.1136/jitc-2021-002662).

HW and XT are joint first authors.

Z-ZY and SMA are joint senior authors.

Accepted 02 June 2021

[1]Department of Immunology, Medical College, China Three Gorges University, Yichang, Hubei, People's Republic of China
[2]Division of Hematology and Internal Medicine, Mayo Clinic, Rochester, MN, USA

Correspondence to
Dr Zhi-Zhang Yang;
yang.zhizhang@mayo.edu

Dr Stephen M Ansell;
ansell.stephen@mayo.edu

ABSTRACT

Background CD8$^+$ T-lymphocyte subsets defined by killer lectin-like receptor G1 (KLRG1) and CD127 expression have been reported to have an important role in infection, but their role in the setting of lymphoid malignancies, specifically follicular lymphoma (FL), has not been studied.

Methods To characterize the phenotype of KLRG1/CD127-defined CD8$^+$ subsets, surface and intracellular markers were measured by flow cytometry and Cytometry by time of flight (CyTOF), and the transcriptional profile of these cells was determined by CITE-Seq (Cellular Indexing of Transcriptomes and Epitopes by Sequencing). The functional capacity of each subset was determined, as was their impact on overall survival (OS) and event-free survival (EFS) of patients with FL.

Results We found that intratumoral CD8$^+$ cells in FL are skewed toward effector cell subsets, particularly KLRG$^+$CD127$^-$ and KLRG1$^-$CD127$^-$ cells over memory cell subsets, such as KLRG1$^-$CD127$^+$ and KLRG1$^+$CD127$^+$ cells. While effector subsets exhibited increased capacity to produce cytokines/granules when compared with memory subsets, their proliferative capacity and viability were found to be substantially inferior. Clinically, a skewed distribution of intratumoral CD8$^+$ T cells favoring effector subtypes was associated with an inferior outcome in patients with FL. Increased numbers of CD127$^+$KLRG1$^-$ and CD127$^+$KLRG1$^+$ were significantly associated with a favorable OS and EFS, while CD127$^-$KLRG1$^-$ correlated with a poor EFS and OS in patients with FL. Furthermore, we demonstrated that interleukin (IL)-15 promotes CD127$^-$KLRG1$^+$ cell development in the presence of dendritic cells via a phosphoinositide 3-kinase (PI3K)-dependent mechanism, and treatment of CD8$^+$ T cells with a PI3K inhibitor downregulated the transcription factors responsible for CD127$^-$KLRG1$^+$ differentiation.

Conclusions Taken together, these results reveal not only a biological and prognostic role for KLRG1/CD127-defined CD8$^+$ subsets in FL but also a potential role for PI3K inhibitors to manipulate the differentiation of CD8$^+$ T cells, thereby promoting a more effective antitumor immune response.

INTRODUCTION

Follicular lymphoma (FL) is the second most common type of non-Hodgkin's lymphoma and is characterized by the presence of abundant T cells in the tumor microenvironment.[1 2] The T cell–mediated immune response has a profound impact on patient outcome.[3–11] However, T cell–mediated immunotherapy including immune checkpoint blockade has shown limited therapeutic benefit in FL and the underlying mechanism remains largely unknown.[12]

CD8$^+$ T cells play a crucial role in the fight against infection and cancer due to their ability to lyse infected or malignant cells.[13 14] During acute infection, antigen-specific CD8$^+$ T cells rapidly expand and differentiate into effector cells to clear the infection. Following expansion, most of the effector cells die, leaving behind a small population that is capable of long-term survival and which protects the host from a subsequent infectious challenge by the same pathogen. During differentiation, effector CD8$^+$ T cells gain expression of killer lectin-like receptor G1 (KLRG1) and enter a pathway ultimately ending in cell death.[15] Some effector CD8$^+$ T cells upregulate or retain expression of interleukin (IL)-7 receptor α (CD127) and differentiate into memory cells. CD8$^+$ T cells expressing KLRG1 but not CD127 are classically defined as 'short-lived effector cells' (CD127$^-$KLRG1$^+$), while CD127$^+$KLRG1$^-$CD8$^+$ T cells are termed 'memory precursor effector cells'.[16] In addition to these two subsets, CD8$^+$ T cells with or without expression of both CD127 and KLRG1 exist and their phenotype and function are largely underexplored.

CD8$^+$ T cells in various stages of differentiation exhibit distinct phenotypes in which their epigenetic and metabolic profiles as well as their intracellular and extracellular cell marker expression render them capable of significant subpopulation variability.[17] As a result, the function of these CD8$^+$ T

cell subsets is expectedly variable as well.[18] In general, however, effector CD8+ T cells are typically functionally active, while CD8+ memory T cells are quiescent but will expand into effector cells in response to an appropriate immune stimulus. However, in circumstances where there is chronic immune stimulation such as chronic infection and cancer, active effector CD8+ cells display a T-cell exhaustion phenotype that eventually diminishes the biological function of cells and renders them predisposed to premature cell death.[19]

While investigated in the context of infection, KLRG1/CD127-defined CD8+ T subsets have not yet been widely explored in the setting of malignancy, and specifically never before in patients with FL. In the present study, therefore, we have sought to determine the prevalence, phenotype, and function of the CD8+ T cell subsets defined by the expression of KLRG1 and CD127 in patients with FL. As a result, for the first time, we demonstrate that these intratumoral CD8+ T subsets have both functional and prognostic relevance in FL.

METHODS

Patient samples

Patients providing written informed consent were eligible for this study if they had a tissue biopsy that on pathologic review showed FL and adequate tissue or peripheral blood to perform the experiments. Peripheral blood mononuclear cells (PBMCs) and tonsils from healthy donors, as well as reactive lymph nodes (rLNs), were used as controls. The use of human tissue samples for this study was approved by the Institutional Review Board of the Mayo Clinic/Mayo Foundation.

Cell isolation and purification

Fresh tumor biopsy specimens from patients with FL and control lymph nodes (LNs) were gently minced over a wire mesh screen to obtain a cell suspension. The cell suspension or peripheral blood from patients or healthy donors was centrifuged over Ficoll Hypaque at 500×g for 20 min to isolate mononuclear cells. CD8+ T cells were isolated using negative selection with CD8 microbeads (StemCell Technologies, Vancouver, Canada). CD8+ subsets were isolated using a flow sorter.

Flow cytometry and intracellular staining

For surface marker detection, 1×10^6 cells were washed in phosphate-buffered saline (PBS) containing 0.5% bovine serum albumin and incubated with fluorochrome-conjugated antibodies (Abs) and analyzed on a flow cytometer. For intracellular staining, cells were stimulated with phorbol myristate acetate (PMA)/ion in the presence of protein transport inhibitor brefeldin A for 4 hours. After fixation and permeabilization, cells were stained with fluorochrome-conjugated Abs for cytokines and analyzed by flow cytometry. For apoptosis detection, cells were cultured with 2 µL Dynabeads® human T-activator CD3/CD28 in 96-well plate at 37°C in the presence of 5% CO_2. On day 3, cells were stained with propidium iodide (PI)/annexin V-Fluorescein isothiocyanate (FITC) and analyzed by flow cytometry. For transcriptional factor (TF) expression detection, cells were fixed and permeabilized with reagents from a Foxp3-staining kit (BioLegend). Cells were then stained with fluorochrome-conjugated Abs against T-bet, Eomes, FOXO1 and TCF-1 plus surface marker Abs and analyzed by flow cytometry.

CFSE labeling and T cell proliferation assay

CD127/KLRG1-defined subsets were sorted by flow cytometry and resuspended at 1×10^6/mL in PBS. A stock solution of Carboxyfluorescein succinimidyl ester (CFSE) (5 mM) was added to the cells for a final concentration of 5 µM. After 10 min at room temperature, cells were washed three times with 10 volumes of PBS containing 10% FBS. CFSE-labeled T cells were cultured with 2 µL Dynabeads® human T-activator CD3/CD28 in 96-well plate at 37°C in the presence of 5% CO_2. Cells were harvested at day 3 or day 7 and analyzed on a flow cytometer.

CyTOF assay

The CyTOF assay was performed according to the manufacturer's instruction. Briefly, 3×10^6 cells were stained with 5 µM Cell-IDTM Cisplatin (Fluidigm, San Francisco, California, USA) for 5 min and quenched with MaxPal Cell Staining Buffer (Fluidigm) using five times the volume of the cell suspension. After centrifugation, cell suspensions (50 µL) were incubated with 5 µL of human Fc-receptor Blocking solution (BioLegend, San Diego, California, USA) for 10 min and 50 µL of pre-mixed antibody cocktail for 30 min. For the staining antibody panel, refer to this publication.[20] After washing, cells were incubated with 1 mL of cell intercalation solution (125 nM MaxPal Intercalator-Ir into 1 mL MaxPal Fix and Pem Buffer, Fluidigm) overnight at 4°C. Cells were centrifuged with MaxPal Water and pelleted. The pelleted cells were suspended with EQ Calibration Beads (Fluidigm) and cell events were acquired by a CyTOF II instrument (Fluidigm).

CyTOF data analysis

The CyTOF data were analyzed using online software (Cytobank) as previously described.[7 21] All the samples were normalized and analyzed simultaneously to account for variability in signal across long acquisition times. A high-level gating strategy was applied simultaneously to all CyTOF files. For specific analysis purposes, we concatenated all sample files to one file. To generate flow files for comparison of distinct populations of interest, we split files by the population and downloaded them into individual files for each sample.

A tSNE map was generated by the t-Distribution Stochastic Neighbor Embedding (tSNE) analysis that makes a pairwise comparison of cellular phenotypes to optimally plot similar cells close to each other and reduces multiple parameters into two dimensions (tSNE1 and tSNE2). For most analysis, we selected equal events

for each sample. Channel (markers) selection was variable depending on cell populations to be clustered. We chose 3000 iterations, perplexity of 30 or 50 and theta of 0.5 as standard tSNE parameters.

For CITRUS (cluster identification, characterization, and regression) analysis, models of significance analysis of microarrays (SAM) and nearest shrunken centroid (PAMR) were selected for association analysis. Abundance was chosen for the cluster characterization and the minimal cluster size was 0.5%. Patients were divided into two groups based on survival (patients dead or alive at last follow-up). CITRUS analysis was performed on $CD8^+$ subsets and we used a number of surface markers (CCR5, CCR6, CCR7, CXCR3, CD5, CD7, CD25, CD26, CD27, CD28, CD57, CD69, CD161, Lymphocyte-activation gene 3 (LAG-3), Inducible T-cell COStimulator (ICOS), T-cell immunoreceptor with immunoglobulin and ITIM domains (TIGIT), T cell immunoglobulin and mucin domain-containing protein 3 (TIM-3), Programmed cell death protein 1 (PD-1), B- and T-lymphocyte attenuator (BTLA), Tumor necrosis factor receptor superfamily member 9 (4-1BB), Human leukocyte antigen-DR (HLA-DR)) to identify clusters that share a unique phenotype. Using correlative (SAM) or predictive (PAMR) methods, CITRUS analysis was able to identify the clusters (populations) that differ significantly between the patient groups by cell abundance (cell events).

The PhenoGraph analysis was performed using FlowJo Plugins. We separated the CD127/KLRG1-defined subsets and exported them as individual FCS files from 82 patients. We then concatenated 82 files into one file for each of these four subsets. Using the software PhenoGraph, we selected a number of surface markers (CD45RA, CCR7, CXCR3, CD26, CD57, CD69, CD161, ICOS, TIGIT, TIM-3, PD-1 and BTLA) to identify clusters for each of these four subsets.

CITE-Seq assay

CITE-Seq was performed according to the manufacturer's instructions (10x Genomics, USA). $CD3^+$ T cells (5×10^5) were resuspended in 50 µL staining buffer and incubated for 10 min with an Fc receptor blocker (Human TruStain FcX, BioLegend, USA). Subsequently, cells were incubated with mixtures of 35 TotalSeq-C antibodies (1 µg per Ab per sample, the panel of antibodies is provided in online supplemental table 3) for 30 min at 4°C. Cells were washed three times in cell staining buffer, followed by centrifugation (350×g 5 min at 4°C). After the final wash, cells were resuspended at appropriate cell concentration (700–1200 cells/µL, viability >90%) in calcium and magnesium free 1× PBS (Corning, USA) containing 0.04% Bovine serum albumin (BSA) (Thermo Fisher Scientific, USA) and run by 10x Genomics applications. The cells were first counted and measured for viability using the Vi-Cell XR Cell Viability Analyzer (Beckman-Coulter). The barcoded Gel Beads were thawed from −80°C and the cDNA master mix was prepared according to the manufacturer's instructions for Chromium Single Cell 5' Library and Gel Bead Kit (10x Genomics). Based on the desired number of cells to be captured for each sample, a volume of live cells was mixed with the cDNA master mix. The cell suspension and master mix, thawed Gel Beads and partitioning oil were added to a Chromium Single Cell A chip. The filled chip was loaded into the Chromium Controller, where each sample was processed and the individual cells within the sample were partitioned into uniquely labeled GEMs (Gel Beads-In-Emulsion). The GEMs were collected from the chip and taken to the bench for reverse transcription, GEM dissolution, and cDNA clean-up. The full-length cDNA was amplified and separated by size selection. The resulting cDNA created a pool of uniquely barcoded molecules used to generate 5′ gene expression libraries (GEX). In addition, the supernatant from the cDNA clean-up step contained amplified DNA from cell surface protein feature barcodes. That DNA was further cleaned and used to create cell surface protein libraries. During library construction, standard Illumina sequencing primers and a unique i7 Sample index (10x Genomics) were added to each cDNA and DNA pool (creating gene expression and feature barcodes libraries, respectively). All cDNA and DNA pools and resulting libraries were measured using Qubit High Sensitivity assays (Thermo Fisher Scientific) and Agilent Bioanalyzer High Sensitivity chips (Agilent).

Gene expression libraries (GEX) were sequenced at a minimum of 50,000 fragment reads per cell and feature barcodes libraries were sequenced at 5000 fragment reads per cell. Sequencing steps followed Illumina's standard protocol using the Illumina cBot and HiSeq 3000/4000 PE Cluster Kit. For GEX, the flow cells were sequenced as 100×2 paired end reads on an Illumina HiSeq 4000 using HiSeq 3000/4000 sequencing kit and HCS V.3.3.52 collection software. For feature barcodes libraries, the flow cells were sequenced as 100×2 paired end reads on an Illumina HiSeq 4000. Base-calling was performed using Illumina's RTA V.2.7.3.

CITE-Seq analysis

The raw 10x CITE-seq data were processed with using Cell Ranger 3.0.0 and was applied default setting of 10x cell ranger pipeline (10x Genomics, USA). Reads were aligned to the human reference sequence GRCh38. After used Cell Ranger multipipeline to analyze FASTQ data derived from Gene Expression data (GEX) that contains the sequence data from the clusters that pass filter on a flow cell and feature barcode (antibody) library from the same GEM Well. The pipeline cellranger aggr was performed for aggregating outputs from several runs of cellranger count or cellranger multiple pipeline. The cellranger aggr pipeline normalizes the individual gene expression and feature barcode (antibody) runs to the same sequencing depth, recomputes the feature-barcode matrices and performs analysis on the concatenated data. After concatenated sequencing data from four lymphoma samples, we used Loupe Browser (https://support.10xgenomics.com/single-cell-gene-expression/software/

downloads/latest#loupe) to analyze the concatenated cloupe file. In Loupe, populations of interest were identified and subjected to comparative analysis by antibody features within the Loupe software, as outlined in the Results section.

GSEA analysis

We used gene set enrichment analysis (GSEA) to explore the difference in transcriptomes among four $CD8^+$ subsets described in the previous study.[22] We implemented GSEA using Cluster Profiler package in R to perform enrichment analysis of gene sets generated from CITE-Seq.[23] The adjusted p value <0.05 was used as the cut-off to determine significance for enrichment score.

Statistics

Statistical analysis was performed using the Student's t test. Significance was determined at $p<0.05$. For non-parametric data, a Mann-Whitney test or Wilcox matched-pairs rank test was performed. Overall survival (OS) or event-free survival (EFS) was measured from the date of diagnosis until death from any cause or until the date of next treatment, respectively. OS or EFS of all patients was estimated using the Kaplan-Meier method. The univariate associations between individual clinical features and survival were determined with the log-rank test. EFS24 (event-free survival at 24 months) achieved or failed was defined as patients who remained in remission or progressed within 24 months of diagnosis. We used the median number of each subset as a cut-off point to delineate patients with high or low content of each of the four $CD8^+$ T subsets. For the datasets with multiple groups, a one-way analysis of variance test was performed to calculate p values. Statistical analysis was performed using software GraphPad Prism V.8 and JMP V.14.

RESULTS

Intratumoral $CD8^+$ T cells are skewed toward $KLRG1^+SP$ over $CD127^+SP$ in patients with FL

To explore the phenotype of intratumoral $CD8^+$ T cell subsets in FL, we first assessed the overall expression of CD127 and KLRG1 using tSNE analysis of CyTOF data from FL tissue samples. We observed that CD127 was expressed on both intratumoral $CD4^+$ and $CD8^+$ T cells in FL indicated by red dots in tSNE plots (figure 1A), accounting for 35.5% and 31.5% of $CD4^+$ and $CD8^+$ T cells, respectively (figure 1B). However, KLRG1 was preferentially expressed on intratumoral $CD8^+$ T cells when compared with intratumoral $CD4^+$ T cells in FL (figure 1A). The number of $KLRG1^+$ cells was 36.4% in $CD8^+$ and 5.5% in $CD4^+$ cells (figure 1B).

Based on differential expression of KLRG1 and CD127, $CD8^+$ T cells were then divided into four subsets: $KLRG1^+CD127^-$ ($KLRG1^+SP$ thereafter, SP: single positive), $CD127^+KLRG1^-$ ($CD127^+SP$ thereafter), $CD127^-KLRG1^-$ (DN thereafter, DN: double negative), $CD127^+KLRG1^+$ (DP thereafter, DP: double positive). The frequency of these four subsets varied among normal tonsil specimens, reactive lymph nodes (rLN) and biopsy specimens from FL (figure 1C). Compared with tonsil and rLN, FL tissues had significantly increased number of $KLRG1^+SP$. In contrast, the number of $CD127^+SP$ was significantly lower in FL than tonsil or rLN (figure 1C). These results suggest that intratumoral CD8 T cells are skewed toward $KLRG1^+SP$ in patients with FL. Supporting this finding, we found that the frequency of $KLRG1^+SP$ was also significantly higher in the peripheral blood of patients with FL (FL-PB) than that of healthy donors (nPB), although we did not see a significant difference of other three $CD8^+$ subsets from PB between healthy donors and FL-PB (figure 1D).

We next determined the relationship between these four subsets and memory cell subsets defined using the canonical classification (central memory (T_{CM}), effector memory (T_{EM}), terminally differentiated memory (T_{EMRA})). As shown in figure 1D, while T_{CM} cells were enriched with $CD127^+SP$ and DP across tissue types (tonsil, rLN and PB from healthy donor or FL) $KLRG1^+SP$ and DN accounted for the majority of T_{EM} cells in FL tissues, with $CD127^+SP$ and DP being major populations in T_{EM} cells from PB of both FL and healthy donors. In terms of T_{EMRA}, DP contributed to a majority of the T_{EMRA} population across tissue types. As a reference, naïve T (T_N) cells were $CD127^+SP$ cells, suggesting a similar phenotype to $CD127^+SP$ (figure 1E).

Intratumoral KLRG1/CD127-defined $CD8^+$ subsets display distinct phenotypes

To determine the phenotypic features of CD127/KLRG1-defined subsets, we separated these four subsets using a gating strategy based on CD127 and KLRG1 expression. We then concatenated all files of CyTOF data from 82 patients with FL into a single file and performed tSNE analysis using markers reflecting T-cell activation, suppression and exhaustion. As shown in figure 2A, the tSNE plots showed that $KLRG1^+SP$ and DN or $CD127^+SP$ and DP, respectively, were relatively similar phenotypically by overall similar tSNE structure (figure 2A). On the other hand, $KLRG1^+SP$ and DN had a tSNE structure markedly different from $CD127^+SP$ and DP (figure 2A). This phenotypic similarity or difference between these subsets was further validated using individual marker expression. Specifically, while the expression level of PD-1, TIGIT, TIM-3, ICOS and BTLA was similar between $KLRG1^+SP$ and DN or $CD127^+SP$ and DP, respectively, $KLRG1^+SP$ and DN expressed significantly higher level of these exhaustion markers than $CD127^+SP$ and DP (figure 2B). This result also indicated that effector cell subsets ($KLRG1^+SP$ and DN) may be more immunologically exhausted than memory cell subsets ($CD127^+SP$ and DP).

One of striking differences between effector and memory subsets was expression of CD26 (adenosine deaminase complexing protein 2). As shown in figure 2B, while it was negligibly expressed by effector subsets ($KLRG1^+SP$ and DN), CD26 was abundantly expressed

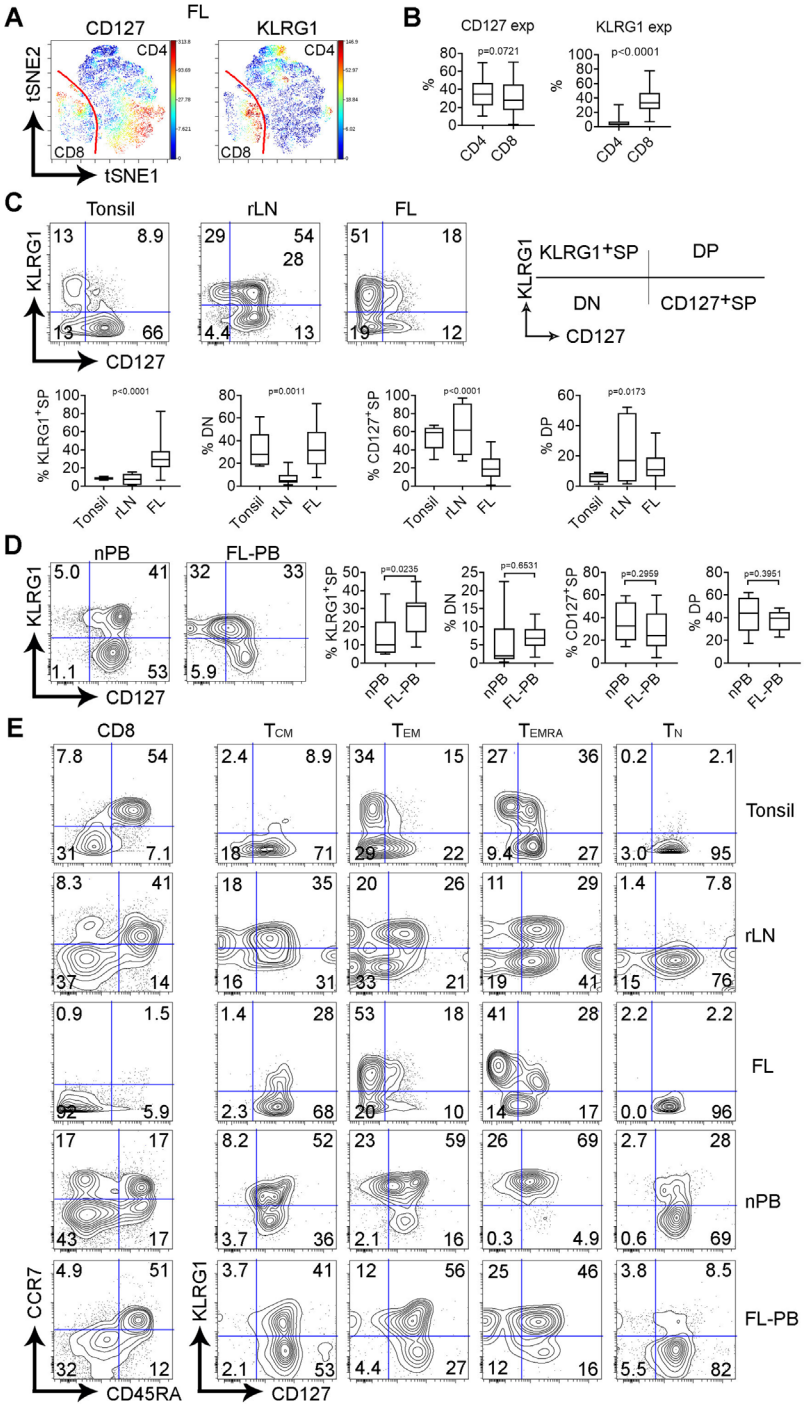

Figure 1 Intratumoral CD8$^+$ T cells are skewed toward KLRG1$^+$SP over CD127$^+$SP in patients with follicular lymphoma (FL). (A) The tSNE (t-Distribution Stochastic Neighbor Embedding) plots showing expression of CD127 and KLRG1 by CD3$^+$ T cells consisting of CD4$^+$ and CD8$^+$ cells from a representative FL sample. (B) Graphs showing the percentages of CD127$^+$ and KLRG1$^+$ cells from CD4$^+$ or CD8$^+$ T cells in FL (n=82). (C, D) Dot plots showing coexpression of CD127 and KLRG1 on CD8$^+$ T cells that defines subsets of KLRG1$^+$SP, DN, CD127$^+$SP and DP from different types of tissues. The percentages of these four subsets from tonsils (tonsil, n=6), reactive lymph nodes (rLNs, n=6), FL biopsy specimens (FL, n=12), peripheral blood from healthy donors (nPB, n=8) and patients with FL (FL-PB, n=8) are shown in graphs below. (E) Dot plots showing expression of CD127 and KLRG1 on T cells of naïve (T_N), central memory (T_{CM}), effector memory (T_{EM}) and terminally differentiated (T_{EMRA}) from tonsils, rLN and FL tissue as well as PBMCs of healthy donors (nPB) and FL (FL-PB). DL, double positive; DN, double negative; KLRG1, killer lectin-like receptor G1. PBMCs, Peripheral blood mononuclear cells.

on a subpopulation from memory subsets (CD127$^+$SP and DP). Given the role of CD26 to promote T cell proliferation by TCR activation, this result suggests that CD127$^+$SP/DP cells have a superior capacity for proliferation when compared with KLRG1$^+$SP/DN cells. As a marker for terminally differentiated cells, we observed that CD57 was

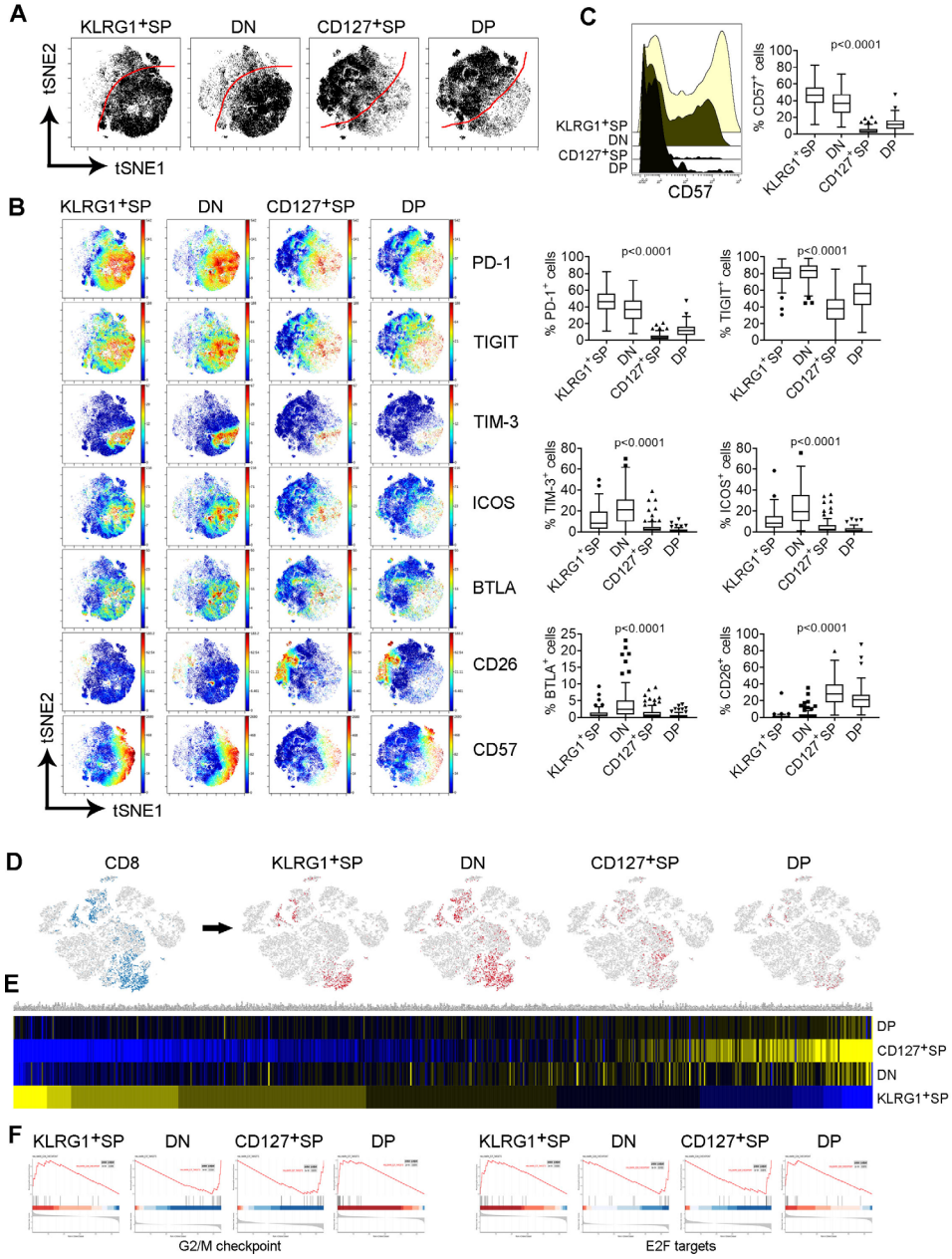

Figure 2 Intratumoral CD8$^+$ subsets display distinct phenotypes. (A) The tSNE (t-Distribution Stochastic Neighbor Embedding) plots showing overall structural presentation of four subsets. Color darkness indicates the intensity of cell events. (B) The tSNE plots showing expression of PD-1, TIGIT, TIM-3, ICOS, BTLA and CD26 on four subsets from a representative follicular lymphoma (FL) sample. The percentage of exhaustion markers from these four subsets from FL was summarized in the graph. (C) Histogram showing CD57 expression on four subsets from a representative FL sample. The percentage of CD57$^+$ four subsets from FL was summarized in the graph. (D) tSNE plots showing distribution of CD8$^+$ and four subsets in CD3$^+$ T cells of FL. The results were obtained using the CITE-Seq (Cellular Indexing of Transcriptomes and Epitopes by Sequencing) assay and analyzed by Loupe Browser (n=4). (E) Heatmap showing global gene expression by four subsets. The gene expression profile was determined using the CITE-Seq assay. (F) The enrichment score curve showing alteration of signaling pathways involving G2/M checkpoints and E2F targets in these four subsets from patients with FL, n=4. The score greater or less than zero indicates an upregulation or downregulation, respectively. These data were generated using gene set enrichment analysis (GSEA). BTLA, B- and T-lymphocyte attenuator; DPP4, CD26, Dipeptidyl-peptidase 4; ICOS, Inducible T-cell costimulator; PD-1, Programmed cell death protein 1;TIGIT, T-cell immunoreceptor with immunoglobulin and ITIM domains; TIM-3, T cell immunoglobulin and mucin domain-containing protein 3.

highly expressed by effector subsets (KLRG1$^+$SP and DN) and minimally expressed by memory cells (CD127$^+$SP and DP), indicating a late stage of differentiation for subsets KLRG1$^+$SP and DN (figure 2C). The expression of other surface markers varied as well among these four subsets (online supplemental figure 1).

Using CITE-Seq (Cellular Indexing of Transcriptomes and Epitopes by Sequencing) technology, we determined

the gene expression of these 4 CD8$^+$ subsets at the single cell level. As shown in figure 2D, these four subsets were distributed to different clusters, suggesting different phenotypes for these four subsets. A heatmap analysis indicated that there was a reciprocal overall gene expression profile between KLRG1$^+$SP and CD127$^+$SP cells. The genes upregulated in KLRG1$^+$SP cells were downregulated in CD127$^+$SP, and vice versa (figure 2E). We next performed a gene set enrichment analysis (GSEA) to explore the altered pathways that are impacted by differentially expressed genes of each of these four subsets. We identified 11, 2, 16 and 8 signaling pathways that were differentially regulated for these four subsets, respectively (online supplemental table 1). A positive or negative enrichment score indicates upregulation or downregulation of a particular pathway, respectively. Among those, signaling pathways of G2/M checkpoints and E2F targets were altered in all of these four subsets with an upregulation in KLRG1$^+$SP and DP cells and downregulation in CD127$^+$SP$^-$ and DN cells, respectively (figure 2F). We observed that some pathways such as TNFα/NFκB and inflammatory response were reciprocally regulated between KLRG1$^+$SP and CD127$^+$SP cells, corresponding to opposite overall gene expression profiles between these two subsets. Of note, the PI3K/AKT pathway was downregulated in CD127$^+$SP cells.

Intratrumoral KLRG1$^+$SP and CD127$^+$SP cells exhibit differing capacity for cytokine production, cell proliferation and survival

We noted that activation using anti-CD3 and anti-CD28 Abs affects expression of CD127 and KLRG1 on CD8$^+$ T cells. As shown in figure 3A, CD8$^+$ T cells treated with 1 µg/mL of anti-CD3 Ab (OKT3) plus anti-CD28 Ab upregulated and downregulated KLRG1 and CD127, respectively. To determine the capacity for proliferation and CK production, we isolated these four subsets by flow sorting and cultured them in anti-CD3 Ab-coated plates with anti-CD28 Ab for 5 days. Cell proliferation and CK production were assessed by CFSE and intracellular staining, respectively. As shown in figure 3B, we observed that KLRG1$^+$SP and CD127$^+$SP cells displayed the lowest and highest capability for cell proliferation, respectively. The number of CFSE^{dim} (proliferated) cells was significantly higher in CD127$^+$SP than KLRG1$^+$SP. These results suggest that CD8$^+$ T cells that differentiate and become KLRG1$^+$SP subsequently lose their proliferative capability.

Next, we determined CK production by these four subsets and found that effector cells (KLRG1$^+$SP and DN) possessed increased capacity for CK production when compared with memory cells (CD127$^+$SP and DP). We showed that KLRG1$^+$SP were functionally superior to CD127$^+$SP as regards the numbers of granule- (granzyme B and perforin) and CK- (IFN-γ and TNF-α) producing cells (figure 3C).

Because these subsets represent different phases of differentiation of CD8$^+$ T cells, we wished to determine the fate of these cells. To test this, we determined the amount of cell death in each subset after activation. Using annexin V (AnV) and propidium iodide (PI) staining, we observed that the memory subsets (CD127$^+$SP and DP) showed greater viability than effector subsets (KLRG1$^+$SP and DN) as the number of AnV$^-$PI$^-$ cells was significantly higher in CD127$^+$SP/DP than KLRG1$^+$SP/DN. In contrast, the number of early (AnV$^+$PI$^-$) and late (AnV$^+$PI$^+$) apoptotic cells was significantly higher in KLRG1$^+$SP/DN than CD127$^+$SP/DP (figure 3D). These results indicate that effector subsets are highly susceptible to apoptosis, consistent with the short-lived nature of KLRG1$^+$SP.

IL-15 promotes the development of KLRG1$^+$SP with the involvement of phosphoinositide 3-kinase pathway

In addition to the characterization of these CD8$^+$ T cell subsets, we next assessed the development of these subsets using an in vitro assay. Activation with autologous dendritic cells (DCs) or anti-CD3/CD28 Ab decreased the numbers of CD127$^+$SP and DP and promoted the development of effector cells that included a substantial increase in DN and a slight enhancement of KLRG1$^+$SP in both naïve and memory cells (figure 4A). This result suggests that activation drives CD8$^+$ memory cells to become more functional effector cells.

We next determined the effect of cytokines on the development of these four subsets. To do this, we activated both memory and naïve CD8$^+$ T cells with autologous DCs in the presence or absence of various cytokines including IL-2, IL-12, IL-15 and IL-18 for 3 days and measured the percentage of each of the four CD8$^+$ subsets. As shown in figure 4B, we observed a reciprocal differentiation pathway between KLRG1$^+$SP/DN and CD127$^+$SP/DP. Activation with DCs increased and decreased the numbers of KLRG1$^+$SP/DN and CD127$^+$SP/DP, respectively. In the presence of cytokines, this effect was further enhanced. We specifically observed that IL-15 significantly enhanced the development of KLRG1$^+$SP and reduced the generation of CD127$^+$SP. Interestingly, driving naïve CD8$^+$ cell differentiation affected the development of DN and CD127$^+$SP in a similar fashion to memory CD8$^+$ cells, but had little effect on KLRG1$^+$SP and DP (figure 4C). While CD8$^+$ T cells activated with mature DCs significantly promoted KLRG1$^+$SP development, we observed that activating pre-sorted CD8$^+$ T cells with anti-CD3/CD28 Abs in the presence of IL-15 produced a minimal increase in KLRG1$^+$SP, suggesting that IL-15-mediated effect on the development of KLRG1$^+$SP requires the presence of DCs (online supplemental figure 2). We measured IL-15 receptor expression on these four subsets and found that CD127$^+$SP cells had highest expression level of IL-15Rα among these four subsets (online supplemental figure 2B). When treated with IL-15, all four subsets showed upregulation of Ki-67 expression (online supplemental figure 2C).

Given the role of IL-15 in the development of KLRG1$^+$SP and the reported role of the phosphoinositide 3-kinase (PI3K) signaling pathway in IL-15-mediated effects, we tested whether blocking the PI3K pathway

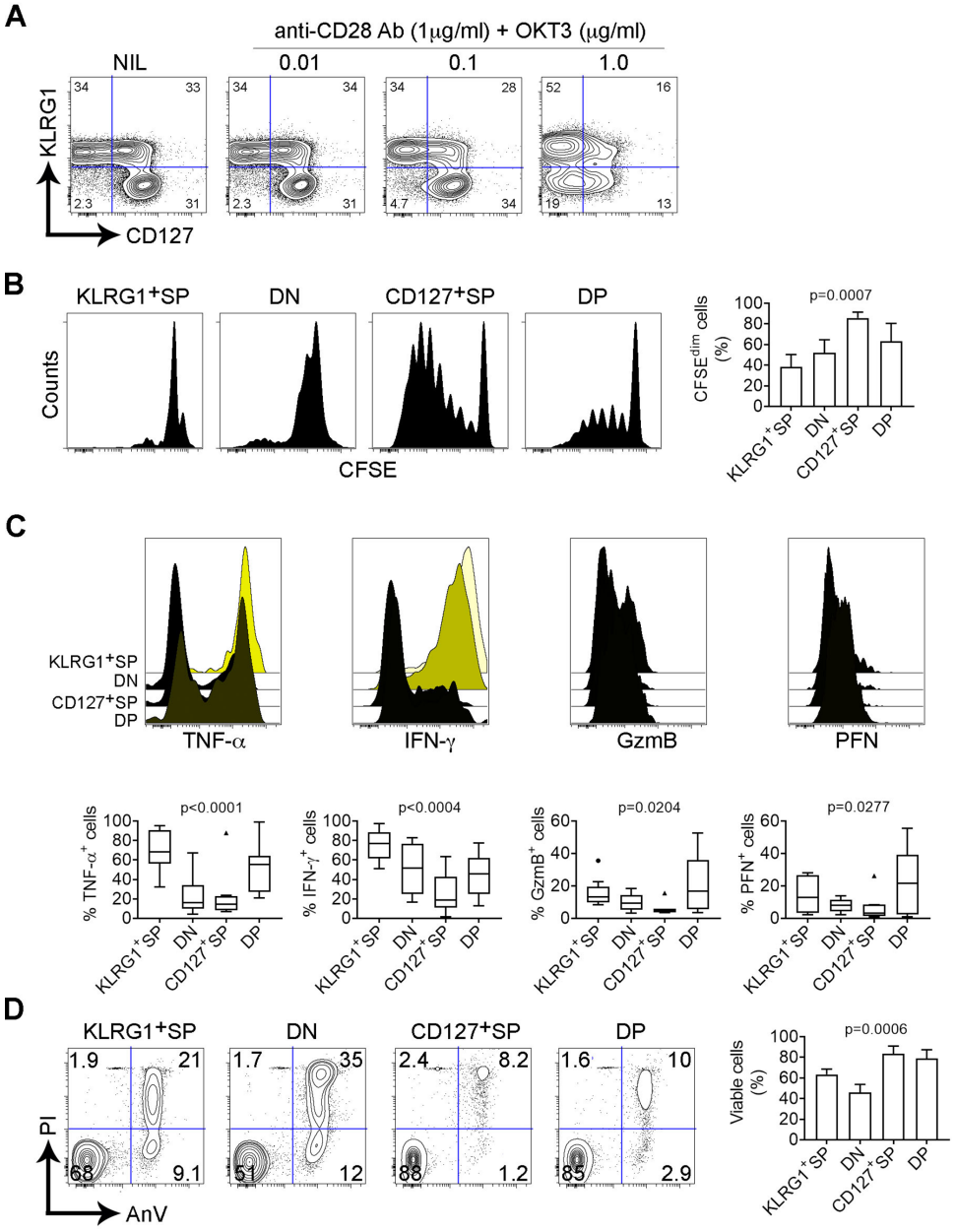

Figure 3 Intratumoral KLRG1$^+$SP and CD127$^+$SP exhibit opposite capacity of cytokine production, cell proliferation and survival. (A) Dot plots showing expression of CD127 and KLRG1 on CD8$^+$ T cells treated with or without anti-CD3 Ab (OKT3) in the presence of anti-CD28 Ab. (B) Histograms showing cell proliferation of these four subsets indicated by CFSE staining. The percentages of proliferated (CFSE^{dim}) cells were summarized in the graph, n=6. (C) Histograms showing cytokine (TNF-α, IFN-γ, GzmB and PFN) production of four subsets by intracellular staining of flow cytometry. The percentages of cytokine-secreting (TNF-α, IFN-γ, GzmB and PFN) cells were summarized in the graph, n=9. (D) Dot plots showing annexin V (AnV) and PI staining of four subsets. The percentage of viable cells (AnV$^-$PI$^-$) was shown in the graph, n=4. Abs, antibodies; DN, double negative; DP, double positive; IFN-γ, interferon-γ; PI, propidium iodide; SP, single positive; TNF-α, tumor necrosis factor-α. CFSE, Carboxyfluorescein succinimidyl ester; GzmB, Granzyme B; PFN, Perforin.

reverses the IL-15-mediated enhancement of KLRG1$^+$SP and reciprocal reduction in CD127$^+$SP. To do this, we treated CD8$^+$ T cells with autologous matured DCs in the presence of IL-15 with or without the PI3Kδ inhibitor (PI3Ki) IC-87114 at various concentrations for 3 days and measured the numbers of CD8$^+$ T cell subsets by flow cytometry. As shown in figure 4D, while IL-15 enhanced the development of KLRG1$^+$SP and DN, the increased number of KLRG1$^+$SP and DN was reversed when CD8$^+$ T cells treated with IC-87114. In contrast, IL-15-mediated inhibition of CD127$^+$SP and DP was restored by incubation with IC-87114. These results suggest the involvement of PI3K signaling pathway in IL-15-mediated regulation of CD8$^+$ T cell differentiation.

It has been shown that Stat5 signaling pathway plays a crucial role in the regulation of CD8$^+$ T cell proliferation and differentiation.[24 25] Therefore, we explored whether blocking the Stat5 pathway with the Stat5 inhibitor,

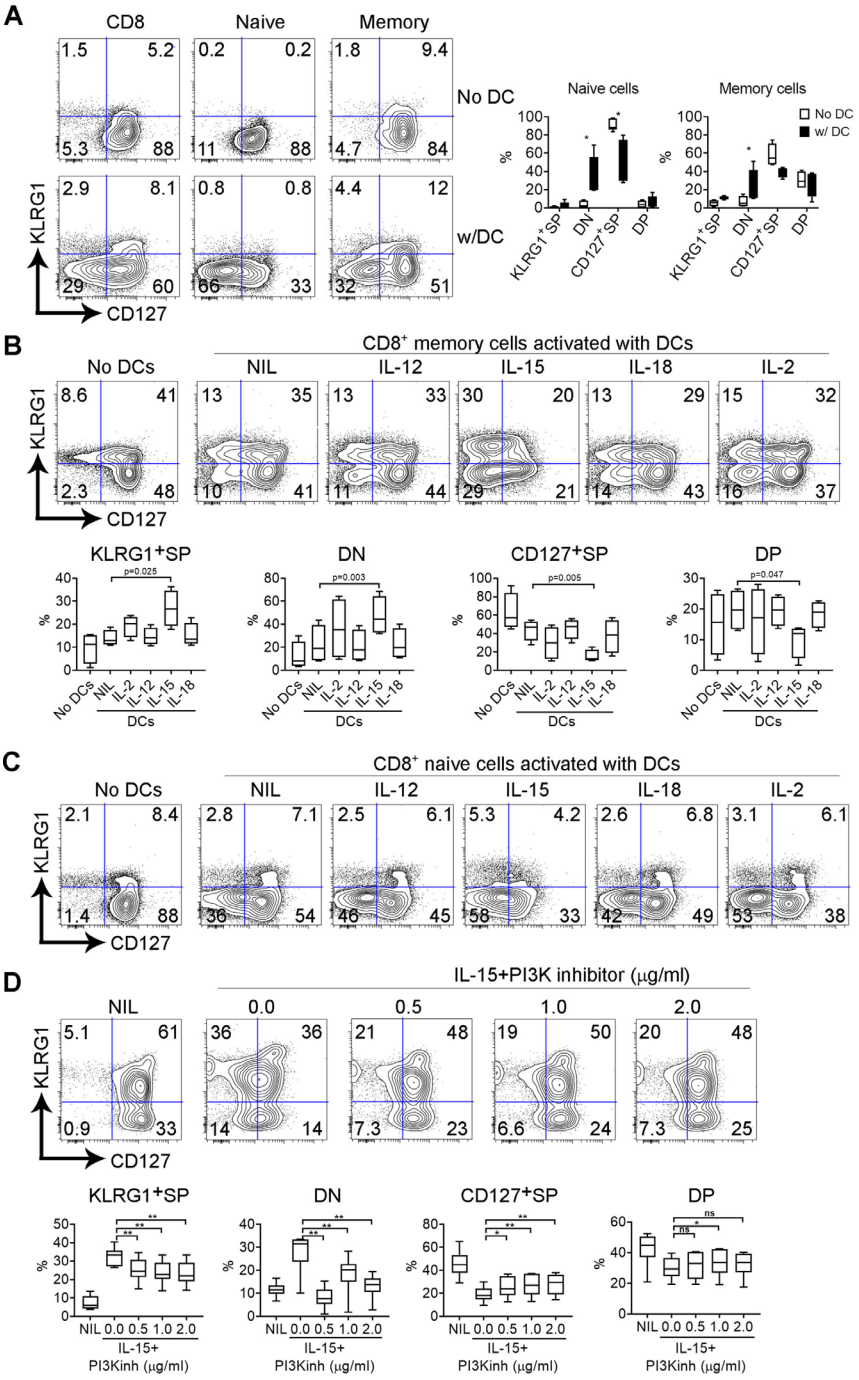

Figure 4 Interleukin (IL)-15 promotes the development of KLRG1$^+$SP with the involvement of phosphoinositide 3-kinase (PI3K) pathway. (A) Dot plots showing coexpression of CD127 and KLRG1 on CD8$^+$, naïve or memory cells stimulated with or without dendritic cells (DCs). The percentages of four subsets induced by DC activation were summarized in the graphs. n=6 for naïve cells, n=4 for memory cells. *p<0.05. (B) Dot plots showing coexpression of CD127 and KLRG1 on CD8$^+$ memory cells activated with DCs in the presence or absence of cytokines (IL-12, IL-15, IL-18 and IL-2). The percentages of four subsets induced by cytokines were summarized in the graphs. NIL indicates cells activated with DCs in the absence of cytokine, n=4. (C) Dot plots showing coexpression of CD127 and KLRG1 on CD8$^+$ naïve cells activated with DCs in the presence or absence of cytokines (IL-12, IL-15, IL-18 and IL-2). (D) Dot plots showing coexpression of CD127 and KLRG1 on CD8$^+$ cells in the presence of IL-15 and with or without PI3K inhibitor (IC-87114) at different doses. The percentages of four subsets induced by IL-15 plus different doses of PI3K inhibitor (IC-87114) were summarized in the graphs, n=6. DN, double negative; DP, double positive; KLRG1, killer lectin-like receptor G1; SP, single positive.

IQDMA, affects the IL-15-mediated CD8$^+$ T cell differentiation into these four subsets. CD8$^+$ cells were activated by autologous mature DCs in the presence of IL-15 with or without IQDMA at various concentrations for 3 days. As shown in online supplemental figure 3A, CD8$^+$ T cells treated with IQDMA resulted in a downregulation of

IL-15-induced KLRG1$^+$SP in a dose-dependent manner. In contrast, the development of DN was upregulated by this inhibitor. While it had no effect on CD127$^+$SP, IQDMA showed an inhibitory effect on DP. We also used a STAT5 siRNA to confirm that inhibition of STAT5 phosphorylation affects IL-15-mediated CD8$^+$ T cell differentiation. As shown in online supplemental figure 3B, STAT5 siRNA transfection blocked phosphorylation of STAT5. CD8$^+$ T cells transfected with STAT5 siRNA resulted in downregulation of IL-15-induced KLRG1$^+$SP (online supplemental figure 3C). In contrast, the development of CD127$^+$SP was upregulated by this blockade. Of note, the blockade of STAT5 pathway is somewhat less effective compared with PI3K blockade of IL-15-mediated CD8$^+$ T cell differentiation.

Regulation of TFs by PI3K pathway blockade contributes to IL-15-mediated development of KLRG1$^+$SP

To further explore the underlying mechanism of the IL-15-mediated effect on KLRG1/CD127-defined subsets, we determined whether various TFs including T-bet, Eomes, FOXO1 and TCF1 were involved. We first measured the expression profile of these four TFs in the intratumoral CD8$^+$ T cell subsets in FL using intracellular staining by flow cytometry. As shown in figure 5A, expression of these four TFs was detectable in intratumoral CD8$^+$ T cells and varied among CD8$^+$ T cell subsets. Compared with other three subsets, DP expressed the highest level of all four TFs. Memory cell subsets (CD127$^+$SP and DP) showed increased expression of FOXO1 and TCF-1 when compared with effector subsets (KLRG1$^+$SP and DN). Of note, CD127$^+$SP expressed the lowest level of Eomes compared with other subsets, contradicting to other reports.[26] Similar findings were seen when calculating the percentage of TF$^+$ cells in four subsets as a measurement (figure 5A).

Next, we determined whether IL-15 regulated expression of these TFs. As shown in figure 5B, activation with DCs enhanced expression of T-bet, Eomes and FOXO1. When treated with IL-15, expression of T-bet, Eomes and FOXO1 was further boosted when compared with cells activated in the absence of IL-15. We observed that TCF-1 expression in CD8$^+$ T cells was inhibited by activation and the number of TCF-1$^+$ cells decreased when cells were treated with IL-15.

Given that the PI3K pathway is involved in IL-15-mediated enhancement of KLRG1$^+$SP, we then tested whether the PI3Ki IC-87114 had effect on IL-15-mediated regulation of these TFs. As shown in figure 5C, upregulation of T-bet, Eomes and FOXO1 expression by IL-15 was reversed when cells were treated with the PI3Ki IC-87114. In contrast, downregulation of TCF-1 expression was reversed by PI3K inhibition. These results suggest that regulation of these TFs is involved in IL-15/PI3K-mediated development of KLRG1$^+$SP and that PI3K inhibition can change phenotype and function of the CD8$^+$ T cells in FL.

Intratumoral CD8$^+$ T cell subsets differentially correlate with patient outcomes in FL

Next, we tested whether these CD8$^+$ T subsets in the tumor microenvironment is associated with patient outcome in FL. Using CyTOF analysis, we measured the numbers of these four subsets in biopsy specimens from a cohort of 82 previously untreated FL patients who had been followed up for long-term outcome.[20] We observed that the intratumoral CD8$^+$ T subsets were differentially represented in patient groups defined by clinical parameters. As shown in figure 6A, the frequency of CD127$^+$SP was significantly lower in patients older than 60 at diagnosis (Dx) compared with patients younger than 60 years. In patients with increased serum lactate dehydrogenase (LDH) at Dx, there were increased and decreased numbers of DN and CD127$^+$SP, respectively, when compared with patients with normal LDH levels. The number of DP decreased in patients who had absolute lymphocyte count (ALC) greater than 0.89×10^9/L at Dx when compared with patients whose ALC is less than 0.89×10^9/L at Dx. In addition, patients who achieved EFS24 had reduced DN and increased DP when compared with patients who failed to achieve EFS24. We did not see a difference in the frequency of these four subsets correlating with other clinical parameters such as histological grade (1/2 vs 3a), stage (I/II vs III/IV), B symptoms (yes vs no), number of nodes (1–3 vs >4) and Follicular Lymphoma International Prognostic Index (FLIPI) scores (1–2 vs 3–5) (data not shown).

As mentioned above, patients with increased LDH had increased and decreased numbers of DN and CD127$^+$SP, respectively. High LDH levels at the time of lymphoma diagnosis reflect increased tumor bulk and predict a less favorable prognosis.[27] The LDH levels mainly measure the metabolic status of lymphoma cells. We therefore evaluated the expression profile of LDH-related genes in each of the CD8$^+$ subsets using CITE-Seq. To generate lactate, glucose goes through a cascade of steps, which is regulated by a variety of enzymes (online supplemental figure 4A). We observed that nine genes associated with enzymes that relate to the LDH cascade were differentially expressed by the four subsets (online supplemental figure 4B). These genes that were upregulated in KLRG1$^+$SP were downregulated in CD127$^+$SP. We found that the oxidative phosphorylation pathway was reciprocally regulated between KLRG1$^+$SP and CD127$^+$SP cells (online supplemental figure 4C) and that the glycolysis pathway was downregulated in CD127$^+$SP cells. This result confirmed an opposite overall LDH-related gene expression profile between these two subsets supporting the differing association with serum LDH values.

We then determined whether the number of these four subsets correlated with EFS and OS in patients with FL. As shown in figure 6B, while KLRG1$^+$SP did not show the correlation with both OS and EFS, increased numbers of CD127$^+$SP and DP were significantly associated with a favorable OS and EFS in this FL patient cohort (p=0.0461 and p=0.0016 for EFS; p=0.021 and p=0.0052 for OS,

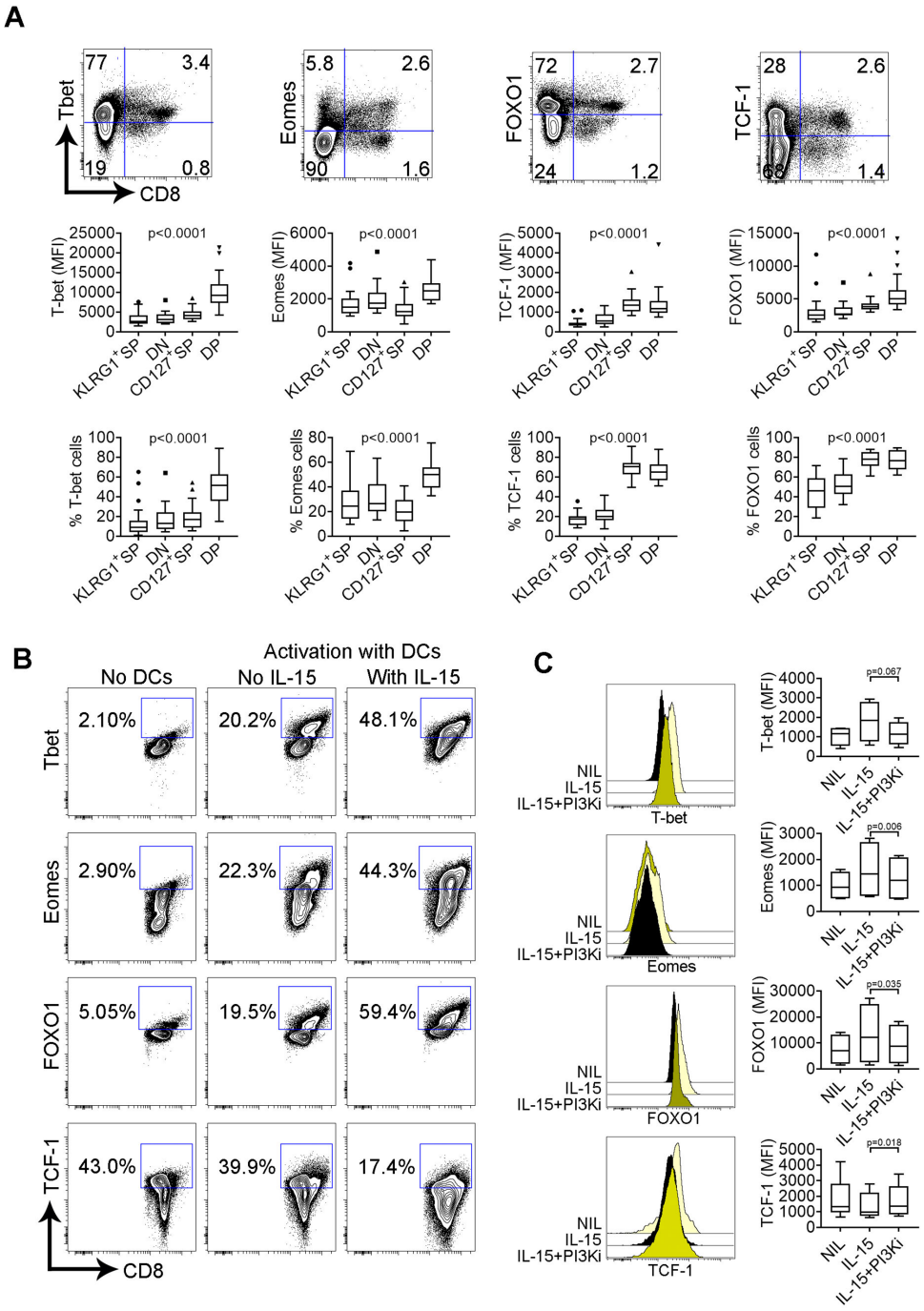

Figure 5 Regulation of transcription factors by phosphoinositide 3-kinase (PI3K) pathway blockade contributes to IL-15-mediated development of KLRG1$^+$SP. (A) Dot plots showing expression of transcriptional factors T-bet, Eomes, FOXO1 or TCF1 on CD8$^+$ T cells from a representative FL sample. The expression level (MFI) of TFs and percentages (%) of T-bet$^+$, Eomes$^+$, FOXO1$^+$ or TCF1$^+$ cells from four subsets were summarized in the graphs, n=13. (B) Dot plots showing expression of transcriptional factors T-bet, Eomes, FOXO1 or TCF1 on resting or activated CD8$^+$ T cells in the presence or absence of IL-15. (C) Histograms showing expression of T-bet, Eomes, FOXO1 or TCF1 on CD8$^+$ T cells treated without or with IL-15 alone or in combination with PI3K inhibitor (IC-87114). The expression level of T-bet, Eomes, FOXO1 or TCF1 with the treatment was summarized in the graphs, n=5. DN, double negative; DP, double positive; FOXO1, Forkhead Box O1; IL, interleukin; KLRG1, killer lectin-like receptor G1; MFI, Mean Fluorescent Intensity; SP, single positive; TCF1, T cell factor ; TF, transcriptional factor.

respectively) using the median number of cells as a cut-off. In contrast, the number of DN showed a significant association with a poor EFS and OS in patients with FL (p=0.0003 and p=0.0383 for EFS and OS, figure 6B). Along with DN, CD127$^+$SP or DP, a univariate analysis showed that age >60 years (p=0.0094), advanced histological grade 3a/b (p=0.0425), increased LDH (p=0.0157) and the presence of B symptoms (p=0.0015) also correlated with overall survival of patients with FL. The multivariate analysis revealed that age, B symptoms, DN and DP, but

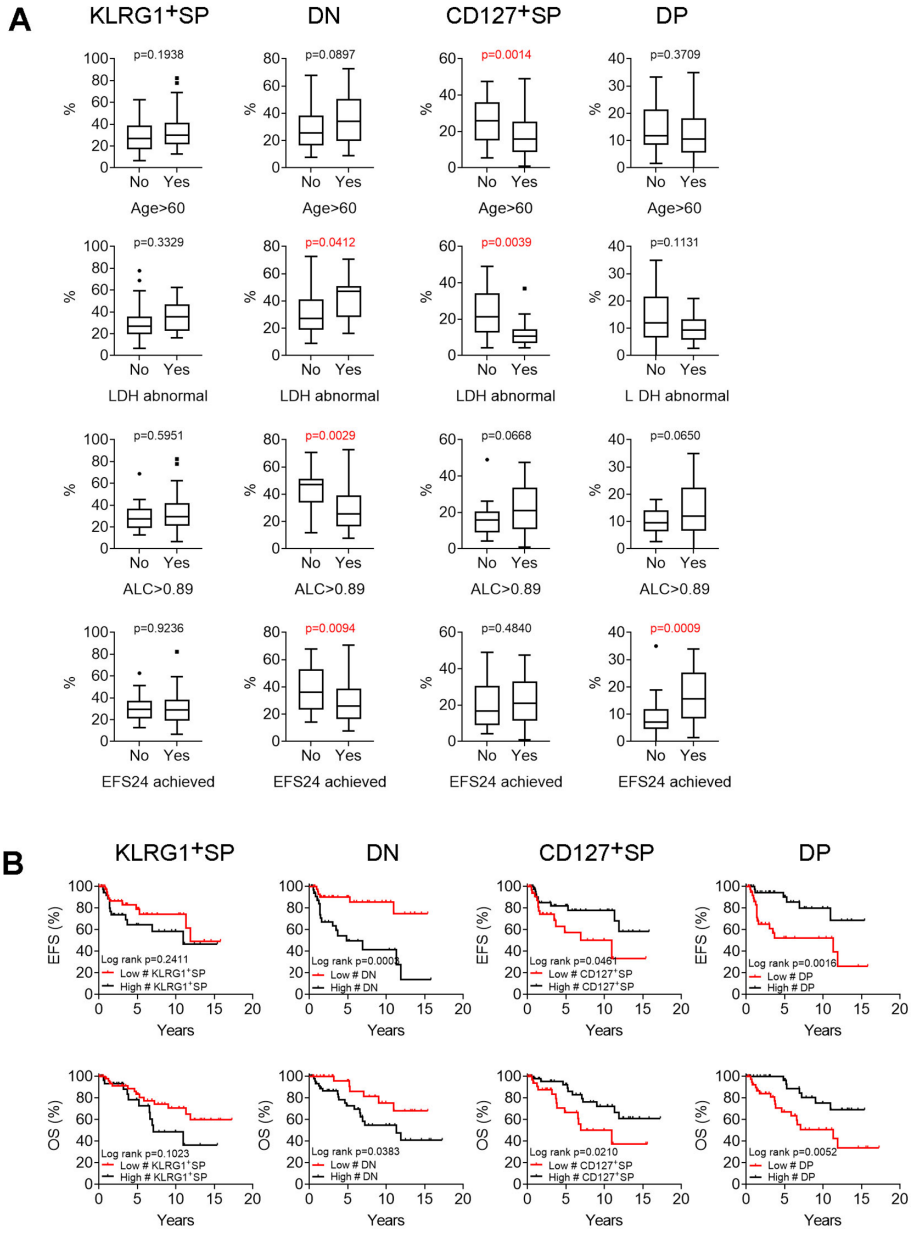

Figure 6 Intratumoral CD8$^+$ T cell subsets differentially correlate to patient outcomes in follicular lymphoma (FL). (A) Graphs showing percentages of four subsets in two patient groups. Patients with FL were grouped using age (older than 60 vs not), lactate dehydrogenase (LDH) level (abnormal vs not), absolute lymphocyte counts (ALC>0.89×10^9/L vs not) and 24-month event-free survival (EFS, achieved vs failed). (B) Kaplan-Meier curves for EFS or overall survival (OS) of patients with FL (n=82) by the number of four subsets. Patients in this cohort received rituximab alone (n=12) or chemoimmunotherapy (n=32). A portion of patients were under observation (n=35). The median follow-up time was 5.27 years (0.02–17.27 years). The cut-point for each subset was determined by using the median number of 82 patient samples. BTLA, B- and T-lymphocyte attenuator; DN, double negative; DP, double positive; HLA-DR, Human leukocyte antigen-DR; ICOS, Inducible T-cell COStimulator; KLRG1, killer lectin-like receptor G1; SP, single positive.

not CD127$^+$SP, were independently associated with OS in this cohort (online supplemental table 2).

Distinct immune signatures contribute to CD8$^+$ subset-associated survival in FL

Given the variable phenotypical and functional capacity and differential survival association of CD8$^+$ subsets in FL, we wanted to explore which immune signature could contribute to the CD8$^+$ subset-associated clinical outcomes. We divided patients into two groups based on survival (24 patients who had died compared with 58 patients who were still alive at the time of last follow-up). Using CITRUS analysis, we identified at least one cluster (red dots) that differed between patients who died or remain alive in the KLRG1/CD127-defined subsets (figure 7A). Two clusters (38,105 and 38,114) were identified from KLRG1$^+$SP in which the abundance (cell numbers) of clusters 38,105 and 38,114 was higher and lower, respectively, in patients who are dead compared

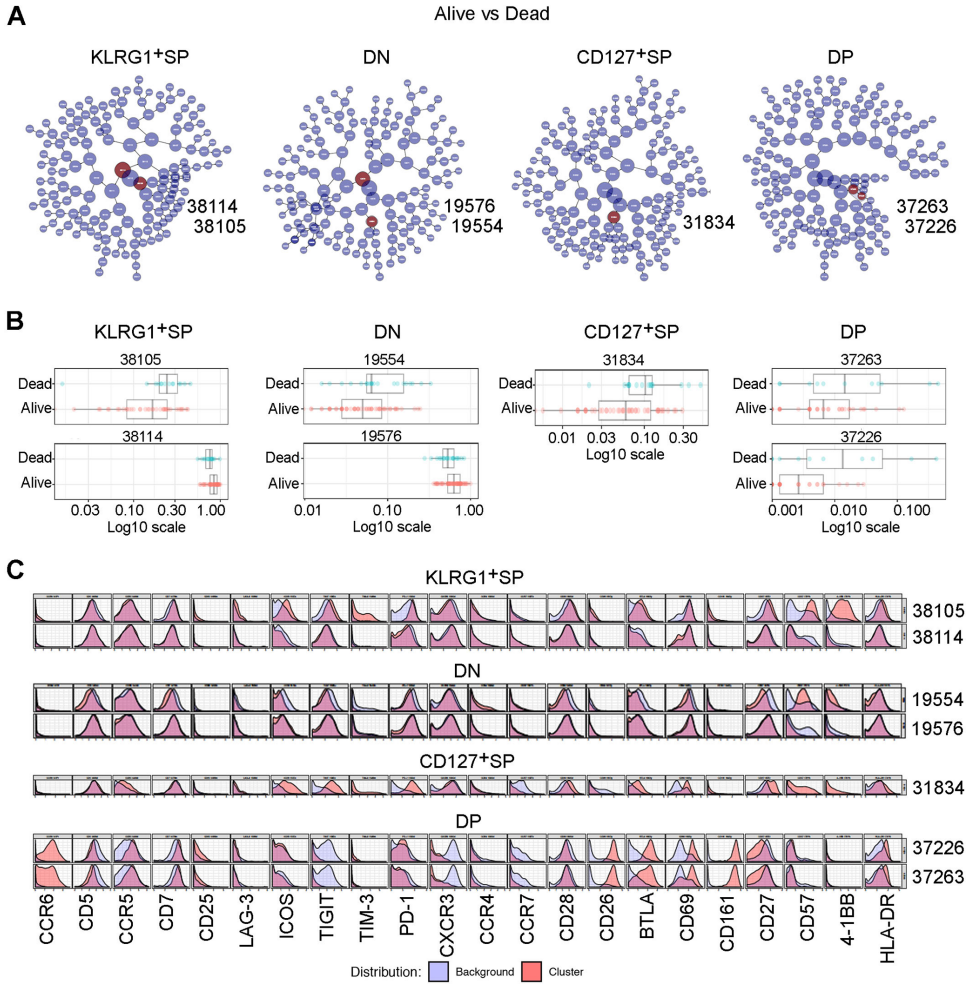

Figure 7 Distinct immune signatures contribute to CD8$^+$ subsets-associated survival in follicular lymphoma (FL). (A) CITRUS plot showing clustering results from patients with FL divided by two groups (patients alive vs dead). Circles in red represent clusters that differed between groups. Number in circles indicates a cluster ID. (B) Graph showing quantitative results of abundance from clusters that are significantly different between patients who dead and who remain alive. (C) Histogram plots showing marker expression by cells from all clusters overlaid on background staining. Expression level of markers was expressed by cluster (red) over background (light blue). CITRUS, cluster identification, characterization, and regression; DN, double negative; DP, double positive; KLRG1, killer lectin-like receptor G1; SP, single positive; TIGIT, T-cell immunoreceptor with immunoglobulin and ITIM domains; TIM-3, T cell immunoglobulin and mucin domain-containing protein 3.

with patients who remain alive (figure 7B). Coincidence with this finding, these two clusters phenotypically differed that clusters 38,105 and 38,114 showed elevated and reduced expression level of TIM-3, PD-1, CD57 and 4-1BB, respectively, when compared with background (red vs gray in histogram, figure 7C). From DN, the abundance of clusters 19,554 and 19,576 was higher and lower in patients who died, respectively, than patients who are alive (figure 7A–B). Consistent with the abundance difference, these two clusters exhibited elevated and reduced expression level of CD57 and 4-1BB, respectively, when compared with background. A single cluster was identified from CD127$^+$SP and was more abundant in patients who are dead than patients who are alive. This cluster showed a typical exhausted phenotype with increased levels of LAG-3, ICOS, TIGIT, TIM-3, PD-1, BTLA, and CD57. From DP, two clusters were both more abundant in patients who died than those who remain alive. These two clusters shared a similar phenotype and had increased levels of CCR6, CCR5, CD26, BTLA, CD161 and reduced levels of TIGIT, CXCR3, CCR7 and CD27 when compared with background (figure 7A–C). These results suggest that while clusters from KLRG1$^+$SP and DN share similar phenotype, clusters from each subset are unique and contribute to patient survival in FL.

Event-free survival at 24 months (EFS24) is an important indicator for patient prognosis in lymphoma. In this regard, we applied CITRUS analysis to patient groups divided by EFS24 (achieved vs failed). As shown in online supplemental figure 5A), we identified 2, 2, 1 and 6 clusters (red dots) that differed between patients who achieved or failed EFS24 in subsets of KLRG1$^+$SP, DN, CD127$^+$SP and DP, respectively. Two clusters (35,313 and 35,317) were identified from KLRG1$^+$SP in which the abundance of clusters 35,313 and 35,317 was higher and lower, respectively, in patients who failed EFS24

compared with patients who achieved EFS24 (online supplemental figure 5B). These two clusters phenotypically differed in that clusters 35,313 and 35,317 showed elevated and reduced expression levels of PD-1, CD57, BTLA and 4-1BB, respectively, compared with background (red vs gray in histogram) (online supplemental figure 5C. For DN, the abundance of clusters 37,376 and 37,378 was higher and lower in patients who failed EFS24, respectively, than patients who achieved EFS24 (online supplemental figure 5A,B). These two clusters exhibited elevated and reduced expression levels of CD57 and 4-1BB, respectively, when compared with background. A single cluster was identified from CD127$^+$SP and was more abundant in patients who failed EFS24 than patients who achieved EFS24. This cluster showed a phenotype with increased levels of ICOS, TIGIT, PD-1, CD69, BTLA, and decreased levels of CCR7, CD45RA, CD26. From DP, five out of six clusters were more abundant in patients who failed EFS24 than those who achieved EFS24. These five clusters shared a similar phenotype and had increased levels of PD-1 and decreased levels of CD45RA. Cluster 12,091 showed increased levels of CD57 and 4-1BB. In contrast, cluster 12,098 was more abundant in patients who achieved EFS24 and showed decreased levels of PD-1, TIGIT and increased levels of CD45RA, CD26 (online supplemental figure 5A–C).

Using PhenoGraph, we identified 17 clusters of intratumoral CD8$^+$ T cells (online supplemental figure 6). These clusters were differentially distributed among CD127/KLRG1-defined subsets. For example, cluster 2 (C2) was abundant in KLRG1$^+$SP and DN, but rarely seen in CD127$^+$SP and DP. In contrast, C6 was enriched in CD127$^+$SP, but negligible in KLRG1$^+$SP (online supplemental figure 6A). Phenotypic analysis showed that cells from C2 expressed increased levels of CD69, TIGIT, PD-1 and CD57 and decreased expression of CD26, CD45RA and CCR7 when compared with cells from C6 (online supplemental figure 6B).

DISCUSSION

There is no doubt that CD8$^+$ T cells play a crucial role in antitumor immunity. However, mechanisms that make CD8$^+$ T cells functionally incompetent exist in the tumor microenvironment. These mechanisms include other cellular subsets (such as T_{reg} cells)[28] or soluble factors (inhibitory cytokines)[29] that result in immune suppression, T cell exhaustion[30 31] and terminal differentiation,[32] resulting in an ineffective antitumor response. Based on expression of CD127 and KLRG1, CD8$^+$ T cells can be divided into four subsets, in various stages of differentiation, that belong to either effector (KLRG1$^+$SP and DN) or memory (CD127$^+$SP and DP) cellular subtypes. While KLRG1$^+$SP and CD127$^+$SP have been previously studied,[33 34] the DN and DP subsets are not well described. In FL, we observed that intratumoral CD8$^+$ T cells are skewed toward an effector rather than memory cell type as the numbers of KLRG1$^+$SP were significantly higher in FL than benign tissues. In contrast, the numbers of CD127$^+$SP were lower in FL than control tissues. This finding suggests persistent, but ineffective, immune activation in the tumor microenvironment of FL, as the completion of an effective immune response would be expected to result in a reduced number of effector cells with an increased number of memory cells.[35 36] The increased prevalence of KLRG1$^+$SP in FL suggests persistent antigenic stimulation without eradication of the malignant clone.

Supporting the contention that persistence of effector cells is indicative of an ineffective antitumor response, we found that increased numbers of effector CD8$^+$ T cells in the initial diagnostic biopsies of patients with FL were associated with an inferior clinical outcome in FL. Interestingly, the effector subsets, especially DN, were associated with a poor survival despite these cells have increased capacity to produce cytokines and granules. These cells, however, have a decreased proliferative capacity and increased predisposition to apoptosis, suggesting that they may be less effective in the antitumor immune response. In contrast, the memory subsets (CD127$^+$SP and DP) correlated with a better survival, suggesting that their phenotypic plasticity and maintenance of function are more useful in suppressing the malignant B-cells.

Many factors are involved in the regulation of CD8$^+$ T cell differentiation that affects the development of these CD8$^+$ T subsets. We found that activation alters the development of DN, CD127$^+$SP and DP by increasing the number of DN and decreasing CD127$^+$SP and DP, respectively, but has little effect on KLRG1$^+$SP. Furthermore, we observed that IL-15 promotes the development of KLRG1$^+$SP, consistent with other studies.[34 37 38] We also found that IL-15-mediated promotion of KLRG1$^+$SP generation is dependent on the presence of DCs. This finding is similar to a previous study suggesting that DCs, especially IL-15Rα^+ DCs, drive CD8 T-cell homeostasis via IL-15 transpresentation thereby upregulating KLRG1$^+$CD27$^-$ CD8 T cells.[39]

The signaling pathways triggered by engagement of IL-15 and its receptor are therefore important for the maintenance of memory T cells.[40 41] Among these signaling pathways, we found that the PI3K pathway is central to IL-15-mediated regulation of CD8$^+$ T cell development. In the presence of a PI3K inhibitor IC-87114, the IL-15-mediated increase in KLRG1$^+$SP and DN differentiation and downregulation of CD127$^+$SP and DP development was reversed. While this is the first time that the role of PI3K signaling pathway in the regulation of CD8$^+$ T subsets has been described, previous studies have found that the PI3K pathway is involved in IL-15-mediated CD8$^+$ T cell survival overall.[42 43] Our results suggest that PI3K inhibitors may have a beneficial therapeutic effect[44 45] in FL by promoting differentiation of CD8$^+$ cells toward a memory phenotype, which is associated with a better outcome, and away from an effector phenotype, which is associated with an ineffective antitumor immune response.

Supporting this, we observed that IL-15-mediated CD8+ subset regulation correlates with changes in the expression of various transcriptional factors (TFs). These TFs include T-bet, Eomes, FOXO1 and TCF1, each of which are essential for CD8+ T cell differentiation either alone or in combination.[46–50] These TFs are differentially and constitutively expressed by intratumoral CD8+ T subsets from FL with higher expression of FOXO1 and TCF1 in memory cells (CD127+SP/DP) than effector cells (KLRG1+SP/DN). However, we found that the expression profile of T-bet and Eomes in CD8+ T subsets in lymphoma is different from that described in other studies using cells obtained from patients with infection[26] in which T-bet and Eomes are highly expressed in KLRG1+SP and CD127+SP, respectively. This difference may be due to different immune signals in the tumor microenvironment and therefore a different immune response. We do show, however, that treatment of CD8+ cells with a PI3K inhibitor, even in the presence of IL-15, restores an overall transcription factor profile that favors differentiation of CD8+ T-cells toward cells with a memory phenotype.

In summary, by comparing the frequency of intratumoral CD8+ T subsets defined by KLRG1 and CD127 to that in normal tissues, we observe that intratumoral CD8+ T cells in patients with FL are skewed toward cells with an effector phenotype of KLRG1+SP over those with a memory phenotype of CD127+SP. While each of these CD8+ subsets exhibit a distinct phenotype and have functional differences, we find that cells with an effector phenotype are less able to proliferate and are less likely to persist, and therefore are associated with an inferior clinical outcome in FL. Treatment with a PI3K inhibitor, however, regulates the transcription factors responsible for CD8+ T-cell differentiation and promotes the differentiation of cells with a memory phenotype. These findings suggest that modulation of CD8+ T-cell differentiation in FL may promote a more effective antitumor immune response and thereby improve the clinical outcome of patients with lymphoma.

Acknowledgements We thank Rakhshan Rohakhtar Fariborz, Vernadette Simon, MS, and other colleagues in Mayo Clinic Medical Genome Facility Genome Analysis Core for performing the CITE-Seq assay. We appreciate the Mayo Immune Monitoring Core for the assistance with the CyTOF analysis.

Contributors HJK and XT performed experiments and analyzed data; HJK and SJ performed experiments; JCP, JCV and AJN analyzed data; Z-ZY and SMA designed the research, analyzed data, and wrote the paper.

Funding The Jaime Erin Follicular Lymphoma Consortium, Department of Defense (W81XWH1810650), National Institutes of Health (P50 CA97274), and the Predolin Foundation.

Competing interests None declared.

Patient consent for publication Not required.

Provenance and peer review Not commissioned; externally peer reviewed.

Data availability statement Data are available on reasonable request.

ORCID iD

Zhi-Zhang Yang http://orcid.org/0000-0002-1468-2300

REFERENCES

1 Sugimoto T, Watanabe T. Follicular lymphoma: the role of the tumor microenvironment in prognosis. *J Clin Exp Hematop* 2016;56:1–19.
2 Yang Z-Z, Ansell SM. The tumor microenvironment in follicular lymphoma. *Clin Adv Hematol Oncol* 2012;10:810–8.
3 Yang Z-Z, Grote DM, Ziesmer SC, *et al*. PD-1 expression defines two distinct T-cell sub-populations in follicular lymphoma that differentially impact patient survival. *Blood Cancer J* 2015;5:e281.
4 Carreras J, Lopez-Guillermo A, Roncador G, *et al*. High numbers of tumor-infiltrating programmed cell death 1-positive regulatory lymphocytes are associated with improved overall survival in follicular lymphoma. *J Clin Oncol* 2009;27:1470–6.
5 Yang Z-Z, Novak AJ, Stenson MJ, *et al*. Intratumoral CD4+CD25+ regulatory T-cell-mediated suppression of infiltrating CD4+ T cells in B-cell non-Hodgkin lymphoma. *Blood* 2006;107:3639–46.
6 Wahlin BE, Aggarwal M, Montes-Moreno S, *et al*. A unifying microenvironment model in follicular lymphoma: outcome is predicted by programmed death-1--positive, regulatory, cytotoxic, and helper T cells and macrophages. *Clin Cancer Res* 2010;16:637–50.
7 Yang Z-Z, Kim HJ, Villasboas JC, *et al*. Mass Cytometry Analysis Reveals that Specific Intratumoral CD4+ T Cell Subsets Correlate with Patient Survival in Follicular Lymphoma. *Cell Rep* 2019;26:2178–93.
8 Glas AM, Knoops L, Delahaye L, *et al*. Gene-expression and immunohistochemical study of specific T-cell subsets and accessory cell types in the transformation and prognosis of follicular lymphoma. *J Clin Oncol* 2007;25:390–8.
9 Yang Z-Z, Novak AJ, Ziesmer SC, *et al*. CD70+ non-Hodgkin lymphoma B cells induce FOXP3 expression and regulatory function in intratumoral CD4+CD25 T cells. *Blood* 2007;110:2537–44.
10 Yang Z-Z, Novak AJ, Ziesmer SC, *et al*. Malignant B cells skew the balance of regulatory T cells and Th17 cells in B-cell non-Hodgkin's lymphoma. *Cancer Res* 2009;69:5522–30.
11 Carreras J, Lopez-Guillermo A, Fox BC, *et al*. High numbers of tumor-infiltrating FOXP3-positive regulatory T cells are associated with improved overall survival in follicular lymphoma. *Blood* 2006;108:2957–64.
12 Lesokhin AM, Ansell SM, Armand P, *et al*. Nivolumab in patients with relapsed or refractory hematologic malignancy: preliminary results of a phase Ib study. *J Clin Oncol* 2016;34:2698–704.
13 Joshi NS, Kaech SM. Effector CD8 T cell development: a balancing act between memory cell potential and terminal differentiation. *J Immunol* 2008;180:1309–15.
14 Hope JL, Stairiker CJ, Bae E-A, *et al*. Striking a Balance-Cellular and molecular drivers of memory T cell development and responses to chronic stimulation. *Front Immunol* 2019;10:1595.
15 Martin MD, Badovinac VP. Defining memory CD8 T cell. *Front Immunol* 2018;9:2692.
16 Backer RA, Hombrink P, Helbig C, *et al*. The fate choice between effector and memory T cell lineages: asymmetry, signal integration, and feedback to create bistability. *Adv Immunol* 2018;137:43–82.
17 Henning AN, Roychoudhuri R, Restifo NP. Epigenetic control of CD8+ T cell differentiation. *Nat Rev Immunol* 2018;18:340–56.
18 Baumann FM, Yuzefpolskiy Y, Sarkar S, *et al*. Dicer regulates the balance of short-lived effector and long-lived memory CD8 T cell lineages. *PLoS One* 2016;11:e0162674.
19 Pauken KE, Wherry EJ. Overcoming T cell exhaustion in infection and cancer. *Trends Immunol* 2015;36:265–76.
20 Yang Z-Z, Kim HJ, Wu H, *et al*. Tigit expression is associated with T-cell suppression and exhaustion and predicts clinical outcome and anti-PD-1 response in follicular lymphoma. *Clin Cancer Res* 2020;26:5217–31.

21 Kotecha N, Krutzik PO, Irish JM. Web-Based analysis and publication of flow cytometry experiments. *Curr Protoc Cytom* 2010;Chapter 10:Unit10 17.
22 Subramanian A, Tamayo P, Mootha VK, *et al*. Gene set enrichment analysis: a knowledge-based approach for interpreting genome-wide expression profiles. *Proc Natl Acad Sci U S A* 2005;102:15545–50.
23 Yu G, Wang L-G, Han Y, *et al*. clusterProfiler: an R package for comparing biological themes among gene clusters. *OMICS* 2012;16:284–7.
24 Grange M, Giordano M, Mas A, *et al*. Control of CD8 T cell proliferation and terminal differentiation by active STAT5 and CDKN2A/CDKN2B. *Immunology* 2015;145:543–57.
25 Verdeil G, Puthier D, Nguyen C, *et al*. Stat5-Mediated signals sustain a TCR-initiated gene expression program toward differentiation of CD8 T cell effectors. *J Immunol* 2006;176:4834–42.
26 Cox MA, Harrington LE, Zajac AJ. Cytokines and the inception of CD8 T cell responses. *Trends Immunol* 2011;32:180–6.
27 Fasola G, Fanin R, Gherlinzoni F, *et al*. Serum LDH concentration in non-Hodgkin's lymphomas. Relationship to histologic type, tumor mass, and presentation features. *Acta Haematol* 1984;72:231–8.
28 Yang Z-Z, Novak AJ, Ziesmer SC, *et al*. Attenuation of CD8(+) T-cell function by CD4(+)CD25(+) regulatory T cells in B-cell non-Hodgkin's lymphoma. *Cancer Res* 2006;66:10145–52.
29 Yang Z-Z, Grote DM, Ziesmer SC, *et al*. Soluble and membrane-bound TGF-β-mediated regulation of intratumoral T cell differentiation and function in B-cell non-Hodgkin lymphoma. *PLoS One* 2013;8:e59456.
30 Yang Z-Z, Grote DM, Ziesmer SC, *et al*. Il-12 upregulates Tim-3 expression and induces T cell exhaustion in patients with follicular B cell non-Hodgkin lymphoma. *J Clin Invest* 2012;122:1271–82.
31 Yang Z-Z, Kim HJ, Villasboas JC, *et al*. Expression of LAG-3 defines exhaustion of intratumoral PD-1$^+$ T cells and correlates with poor outcome in follicular lymphoma. *Oncotarget* 2017;8:61425–39.
32 Yang Z-Z, Grote DM, Xiu B, *et al*. TGF-β upregulates CD70 expression and induces exhaustion of effector memory T cells in B-cell non-Hodgkin's lymphoma. *Leukemia* 2014;28:1872–84.
33 Remmerswaal EBM, Hombrink P, Nota B, *et al*. Expression of IL-7Rα and KLRG1 defines functionally distinct CD8$^+$ T-cell populations in humans. *Eur J Immunol* 2019;49:694–708.
34 Herndler-Brandstetter D, Ishigame H, Shinnakasu R, *et al*. KLRG1$^+$ Effector CD8$^+$ T Cells Lose KLRG1, Differentiate into All Memory T Cell Lineages, and Convey Enhanced Protective Immunity. *Immunity* 2018;48:716–29.
35 Kalia V, Sarkar S, Ahmed R. Cd8 T-cell memory differentiation during acute and chronic viral infections. *Adv Exp Med Biol* 2010;684:79–95.
36 Joshi NS, Cui W, Chandele A, *et al*. Inflammation directs memory precursor and short-lived effector CD8(+) T cell fates via the graded expression of T-bet transcription factor. *Immunity* 2007;27:281–95.
37 Rubinstein MP, Lind NA, Purton JF, *et al*. Il-7 and IL-15 differentially regulate CD8+ T-cell subsets during contraction of the immune response. *Blood* 2008;112:3704–12.
38 Mathieu C, Beltra J-C, Charpentier T, *et al*. Il-2 and IL-15 regulate CD8+ memory T-cell differentiation but are dispensable for protective recall responses. *Eur J Immunol* 2015;45:3324–38.
39 Stonier SW, Ma LJ, Castillo EF, *et al*. Dendritic cells drive memory CD8 T-cell homeostasis via IL-15 transpresentation. *Blood* 2008;112:4546–54.
40 Richer MJ, Pewe LL, Hancox LS, *et al*. Inflammatory IL-15 is required for optimal memory T cell responses. *J Clin Invest* 2015;125:3477–90.
41 Berard M, Brandt K, Bulfone-Paus S, *et al*. Il-15 promotes the survival of naive and memory phenotype CD8+ T cells. *J Immunol* 2003;170:5018–26.
42 Hand TW, Cui W, Jung YW, *et al*. Differential effects of Stat5 and PI3K/Akt signaling on effector and memory CD8 T-cell survival. *Proc Natl Acad Sci U S A* 2010;107:16601–6.
43 Kim EH, Suresh M. Role of PI3K/Akt signaling in memory CD8 T cell differentiation. *Front Immunol* 2013;4:20.
44 Yang J, Nie J, Ma X, *et al*. Targeting PI3K in cancer: mechanisms and advances in clinical trials. *Mol Cancer* 2019;18:26.
45 Curran E, Smith SM. Phosphoinositide 3-kinase inhibitors in lymphoma. *Curr Opin Oncol* 2014;26:469–75.
46 Naito T, Tanaka H, Naoe Y, *et al*. Transcriptional control of T-cell development. *Int Immunol* 2011;23:661–8.
47 Kallies A, Good-Jacobson KL. Transcription factor T-bet orchestrates lineage development and function in the immune system. *Trends Immunol* 2017;38:287–97.
48 Intlekofer AM, Takemoto N, Wherry EJ, *et al*. Effector and memory CD8+ T cell fate coupled by T-bet and eomesodermin. *Nat Immunol* 2005;6:1236–44.
49 Zhang L, Tschumi BO, Lopez-Mejia IC, *et al*. Mammalian target of rapamycin complex 2 controls CD8 T cell memory differentiation in a FoxO1-dependent manner. *Cell Rep* 2016;14:1206–17.
50 Danilo M, Chennupati V, Silva JG, *et al*. Suppression of Tcf1 by Inflammatory Cytokines Facilitates Effector CD8 T Cell Differentiation. *Cell Rep* 2018;22:2107–17.